



# Correlation between optical and UV variability of a large sample of quasars

Chengcheng Xin,<sup>1★</sup> Maria Charisi,<sup>2★</sup> Zoltán Haiman<sup>1</sup> and David Schiminovich<sup>1</sup>

<sup>1</sup>*Department of Astronomy, Columbia University, New York, NY 10027, USA*

<sup>2</sup>*TAPIR, California Institute of Technology, Pasadena, CA 91125, USA*

Accepted 2020 April 6. Received 2020 April 1; in original form 2020 January 9

## ABSTRACT

The variability of quasars across multiple wavelengths is a useful probe of physical conditions in active galactic nuclei. In particular, variable accretion rates, instabilities, and reverberation effects in the accretion disc of a supermassive black hole are expected to produce correlated flux variations in ultraviolet (UV) and optical bands. Recent work has further argued that binary quasars should exhibit strongly correlated UV and optical periodicities. Strong UV–optical correlations have indeed been established in small samples of ( $N \lesssim 30$ ) quasars with well-sampled light curves, and have extended the ‘bluer-when-brighter’ trend previously found within the optical bands. Here, we further test the nature of quasar variability by examining the observed-frame UV–optical correlations among bright quasars extracted from the Half Million Quasars (HMQ) catalogue. We identified a large sample of 1315 quasars in HMQ with overlapping UV and optical light curves from the Galaxy Evolution Explorer and the Catalina Real-time Transient Survey, respectively. We find that strong correlations exist in this much larger sample, but we rule out, at  $\sim 95$  per cent confidence, the simple hypothesis that the intrinsic UV and optical variations of all quasars are fully correlated. Our results therefore imply the existence of physical mechanism(s) that can generate uncorrelated optical and UV flux variations.

**Key words:** galaxies: active – quasars: general.

## 1 INTRODUCTION

Quasars are thought to be powered by gas accreted on to supermassive black holes (SMBHs; Lynden-Bell 1969). The black hole is fed by a geometrically thin accretion disc, whose thermal emission is stratified radially, with higher energy radiation arising from the hotter inner regions (e.g. Frank, King & Raine 2002).

A prominent feature of quasars is their variability across multiple wavelengths. Quasars appear to vary on time-scales from minutes to years and their variability has been studied extensively. This is especially true in optical bands, where time-domain surveys have provided large samples of quasar light curves. The variability is stochastic, and well described by random Gaussian fluctuations, whose autocorrelation function obeys the so-called damped random walk (DRW) model (e.g. Kelly, Bechtold & Siemiginowska 2009; Kozłowski et al. 2010; MacLeod et al. 2010; Andrae, Kim & Bailer-Jones 2013; Ivezić & MacLeod 2013; but see Kozłowski 2017; Sánchez-Sáez et al. 2018; Smith et al. 2018 and references therein for discussions on discrepancies from this model). Similar behaviour is also seen in the ultraviolet (UV) band, with generally

larger variability amplitudes (Welsh, Wheatley & Neil 2011; Gezari et al. 2013; Zhu et al. 2016).

The origin of the stochastic variability is currently poorly understood, but in general, fluctuations in the accretion rate (Pereyra et al. 2006; Li & Cao 2008; Schmidt et al. 2012; Ruan et al. 2014), instabilities or inhomogeneities in the accretion disc (e.g. Dexter & Agol 2011), and reprocessing of variable higher energy (X-ray) emission from a hot corona within a few gravitational radii of the central SMBH (George & Fabian 1991; Krolik et al. 1991) could all cause variability in optical and UV bands.

All of the above mechanisms are expected to induce variability that is correlated across wavelengths. Indeed, cross-correlations within the optical bands are well established, with a clear ‘bluer-when-brighter’ trend (Vanden Berk et al. 2004; Wilhite et al. 2005; Schmidt et al. 2012). These interband correlations should be especially useful to constrain physical models, since in the radially stratified discs, the UV and optical emission regions are expected to be spatially well separated and therefore need not necessarily co-vary (e.g. if there are localized temperature fluctuations in an inhomogeneous disc; Dexter & Agol 2011). For example, interband cross-correlations have been used to test whether variability can be fully explained by changes in the accretion rate of a quasi-steady disc, with early work finding consistency (Pereyra et al.

\* E-mail: cx2204@columbia.edu (CX); mcharisi@caltech.edu (MC)

2006), but recent studies finding that accretion rate variations alone cannot fully explain the observed colour variability (Schmidt et al. 2012; Kokubo et al. 2014; Ruan et al. 2014). Likewise, localized temperature fluctuations appear not to be the main driver of optical colour variability (Ruan et al. 2014; Kokubo 2015).

Cross-correlations have also been established between the UV and optical bands (Hung et al. 2016; Edelson et al. 2019). Because UV data are typically sparse, previous studies of the optical-to-UV cross-correlations have been performed only on small samples. For example, Edelson et al. 2019 relied on well-sampled light curves, obtained via intense monitoring of four active galactic nuclei (AGNs) in optical and UV (as well as X-ray) bands with *Swift*. They find strong UV/optical cross-correlations, with time lags (of the order of a  $\tau \sim \text{day}$ ) whose value is larger, but the scaling consistent with  $\tau \propto \lambda^{4/3}$  expected in a radially stratified and centrally illuminated thin disc. Similar results were found by Fausnaugh et al. (2016) for the Seyfert galaxy NGC 5548 with an active nucleus, using ground-based optical monitoring, combined with UV data from the *Hubble Space Telescope* and *Swift*. Hung et al. (2016) analysed the wavelength-dependent variability of 23 AGNs with large optical variability in the Panoramic Survey Telescope and Rapid Response System (Pan-STARRS), combined with two epochs of UV data, separated by approximately a year, in the Galaxy Evolution Explorer (*GALEX*) Time Domain Survey. They found that the UV/optical correlations for 17 out of the 23 quasars are consistent with the variable accretion rate disc model.

Additionally, recent work has identified possibly significant optical periodicity in a small fraction of quasars (Graham et al. 2015; Charisi et al. 2016; Liu, Gezari & Miller 2018). These quasars have been proposed to host binary SMBHs, whose orbital motion is expected to induce periodic variability due to hydrodynamical modulations in the accretion rate (e.g. Hayasaki, Mineshige & Ho 2008; MacFadyen & Milosavljević 2008; Roedig et al. 2011; Shi et al. 2012; D’Orazio, Haiman & MacFadyen 2013; Farris et al. 2014; Muñoz, Miranda & Lai 2019), as well as due to relativistic Doppler boost of the emission from gas bound to individual SMBHs (D’Orazio, Haiman & Schiminovich 2015; Charisi et al. 2018; Xin et al. 2019). The latter effect induces strongly correlated variability in optical and UV bands with amplitudes that depend on the spectral curvature. Given the limited quality of currently available UV light curves, Doppler-boost variability can be confused with the multiwavelength variability of aperiodic single SMBH quasars (Charisi et al. 2018).

In this paper, we complement previous work by examining the observed UV *versus* optical cross-correlations in a large sample of quasars. Our motivation is to assess whether tight correlations are generic and exist in all quasars, or if there are examples of uncorrelated, or only partially correlated optical and UV flux variations. In order to do this, we created a sample of  $> 1000$  quasars, which have adequately sampled and overlapping UV and optical time series, from *GALEX* and Catalina Real-time Transient Survey (*CRTS*), respectively. Our starting point is the Half Million Quasar catalogue (HMQ), which is a compilation of all known quasars in the literature (Flesch 2015). By analysing the covariance between the pairs of light curves, we find that strong correlations exist in this larger sample, but we rule out, at  $\sim 95$  per cent confidence, the simple hypothesis that the intrinsic UV and optical variations of all quasars are fully correlated. Our results therefore imply the existence of physical mechanism(s) that can generate unrelated optical and UV flux variations.

The rest of this paper is organized as follows. In Section 2, we describe our methodology, including the UV and optical quasar

catalogues we used (Section 2.1), the construction of our joint UV + optical sample of 1315 sources (Section 2.2), and our analysis of the light curves, including the computation of the cross-covariance between the noisy and sparsely and heterogeneously sampled pairs of time series (Section 2.3). In Section 3 we present our findings, in the form of the distribution of the cross-correlation coefficients found for the 1315 quasars. These distributions are determined both by intrinsic correlations, as well as the data quality; we compare them with the distributions predicted under different assumptions of the underlying *intrinsic* correlations. In Section 4 we discuss these results, including the impact of the poor sampling, limited baselines, and photometric noise, as well as the possibility of time lags and partial correlations. Finally, we summarize our findings and conclusions in Section 5.

## 2 SAMPLE SELECTION AND DATA ANALYSIS

### 2.1 UV and optical data

In order to study the observed-frame correlation between UV and optical variability in a large sample of quasars, we extract UV and optical light curves from *GALEX* and *CRTS*, respectively. The combination of these two surveys is optimal, because both are all-sky surveys, covering large samples of quasars, the light curves of which have significant temporal overlap.<sup>1</sup>

In particular, *GALEX* (Martin et al. 2005) was the first all-sky survey in the UV band. *GALEX* operated from 2003 to 2012 and provided simultaneous photometric measurements in two UV filters, in the far-UV (1350–1750 Å) and near-UV (1750–2750 Å) bands (hereafter FUV and NUV, respectively). It performed three main surveys (Bianchi, Shiao & Thilker 2017): (i) an all-sky imaging survey (40 000 deg<sup>2</sup>) with a limiting FUV and NUV magnitudes of  $m_{AB} \sim 20$  and  $\sim 21$ , respectively, (ii) a medium imaging survey (1000 deg<sup>2</sup>) with limiting magnitude  $m_{AB} \sim 22.7$  for both FUV and NUV, and (iii) a deep imaging survey (100 deg<sup>2</sup>) with limiting magnitudes  $m_{AB} \sim 24.8, 24.4$  for FUV and NUV. In addition, from 2008 to 2011, *GALEX* performed a time-domain survey (40 deg<sup>2</sup>) with a 2-d cadence (Gezari et al. 2013).

*CRTS* (Drake et al. 2009) is an ongoing time-domain survey, which covers the majority of the sky from declinations of  $-75^\circ$  to  $65^\circ$ , with the exception of the galactic plane, in unfiltered optical light, broadly calibrated in the Johnson *V* band with a limiting magnitude of  $\sim 19$  (for observations with the Siding Springs Survey telescope) to 20 (with the Catalina Sky Survey and Mount Lemmon Survey telescopes). It began operations in 2005 and the most recent data release (Data Release 2), which we use, extends to 2014.<sup>2</sup> *CRTS* covers up to  $\sim 2500$  deg<sup>2</sup> per night and each visit consists of four exposures, separated by 10 min.

### 2.2 Sample selection

Our basic approach is to study as large a population of quasars as possible. For this, we first select the sample based on the UV light curves, and after necessary quality cuts, we cross-correlate

<sup>1</sup>Note that *GALEX* is the only wide and deep time-domain survey in UV, whereas in the optical, Pan-STARRS and the Palomar Transient Factory (PTF) are less ideal for this study, because they began operations after *CRTS*, and their overlap with *GALEX* is more limited.

<sup>2</sup>Even though *CRTS* continues operations, the most recent data are not publicly available.

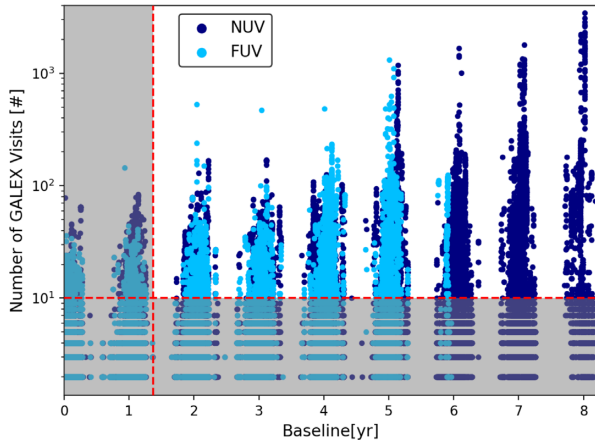


**Figure 1.** The number of *GALEX* visits are shown against the total baseline for the entire NUV and FUV samples, in dark and light blue, respectively. The red dashed lines denote necessary quality cuts on the light curves (i.e. at least 10 visits and baselines of 500 d). These cuts exclude the sources in the shaded area from our final sample.

with *CRTS*. This strategy maximizes the sample of quasars with suitable data, since it optimizes the selection for the UV sample, which typically has lower quality data. We note that even with this strategy, it is still necessary to compromise on the quality of the individual light curves, in order to maintain a large sample.

Our starting sample is the HMQ catalogue (version 4.4; Flesch 2015), which consists of 424 748 spectroscopically confirmed quasars. We extracted sources within 5 arcsec from the input position using the final *GALEX* data release (DR6/7).<sup>3</sup> Of the quasars in the HMQ catalogue, 159 750 have at least one observation in the NUV band. The extracted sample contains a broad population of quasars at various redshifts (up to  $z \approx 5$ ), and NUV magnitudes ( $16 \lesssim m_{AB}(NUV) \lesssim 24$ ), as shown by the dark blue points and curves in Fig. 3.

In Fig. 1, we show the number of observations versus the baseline of the light curves for the entire *GALEX* sample in both the NUV and FUV bands. Here, we define baseline as the interval between the first and last observation, i.e. simply the length of the light curve in years. The typical light curves from *GALEX* are sparse with only a few epochs, but there is a large variety in terms of number of observations and temporal baselines ranging from a few days up to 10 yr, similar to the findings in Welsh et al. (2011). It is also clear that the selected quasars have fewer data points in FUV compared to the NUV band, as expected due to the fact that the FUV detector was operational over a shorter time span. For this reason, in the remainder of this paper, we focus only on the NUV light curves.

In order to avoid possible biases associated with too few observations, we select light curves based on the number of data points. In Fig. 2 (bottom panel), we show the number of quasars remaining in the sample as a function of the minimum allowed number of observations. As expected, requiring more visits results in a declining number of available quasars. We set the minimum required number of *GALEX* visits to 10, which ensures relatively more frequently sampled sources, while maintaining a large sample of 13 087 quasars. In Fig. 2 (top panel), we show the mean NUV magnitude versus the number of *GALEX* visits; the NUV catalogue

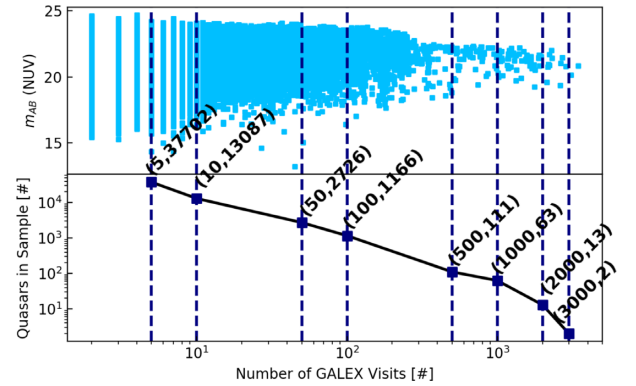


**Figure 2.** The top panel shows the mean NUV magnitude versus the number of *GALEX* visits for each source. The dashed lines mark cuts corresponding to various different minimum number of visits. The bottom panel shows the cuts and the number of quasars left in the sample after each cut, which are indicated with two numbers in the parentheses.

(both initially and after the aforementioned quality cut) consists of quasars with a wide range of mean photometric magnitudes.

Among these 13 087 *GALEX* NUV sources, we exclude light curves with baselines shorter than  $\sim 500$  d. We have found it necessary to exclude these light curves, because for the cross-correlation analysis, we need at least three distinct well-separated epochs.<sup>4</sup> Light curves spanning less than  $\sim 500$  d are typically observed for only two epochs, as can be inferred from the sampling pattern in Fig. 1. In addition, the typical DRW time-scale  $\tau$  is a few 100 d (MacLeod et al. 2010). As a result, in order to fairly sample the light curves, the overlap should cover longer periods for an unbiased measurement of cross-correlations. This additional requirement resulted in a relatively minor cut, eliminating only 900 of the 13 087 quasars.

The remaining 12 187 quasars in the *GALEX* UV catalogue are then cross-matched with their optical counterparts in the *CRTS* catalogue.<sup>5</sup> We extract light curves within 3 arcsec from the HMQ catalogue coordinates, which returns a total of 2840 quasars.

For the cross-correlation analysis, we need spatially and temporally overlapping optical and UV data, which imposes further cuts on the sample. For this, we identified the temporal overlap between the UV and optical light curves of each source, and excluded sources whose NUV light curve did not cover at least three distinct epochs within the optical baseline. Finally, we then excluded sources with unrealistically high virial black hole mass estimates (see Section 2.3.2 below). Overall, these selections result in 1315 high-quality (according to our criteria) pairs of light curves.

In Fig. 3, we show the distribution of redshift and NUV magnitude for the initial sample extracted from *GALEX* along with the final sample of 1315 quasars. The properties of our final sample resemble those of the input parent sample, without introducing significant biases. Specifically, our final sample covers broad ranges of redshifts and magnitudes, similar to those in the original *GALEX* and *CRTS* catalogues. Fig. 3 shows that the redshift distribution of our sample preserves the peak at  $z \approx 1$ , although it also shows that our selection removes sources with higher redshifts, which tend to be dim with

<sup>4</sup>In the UV light curves, we define an epoch as a cluster of time-ordered points separated with gaps smaller than 30 d. While somewhat ad hoc, we have found that in practice, this definition identifies the discrete clusters of data points (e.g.  $\approx 10$  such clusters are seen among the grey points Fig. 5).

<sup>5</sup><http://nessi.cacr.caltech.edu/DataRelease/>

<sup>3</sup><https://asd.gsfc.nasa.gov/archive/galex/>

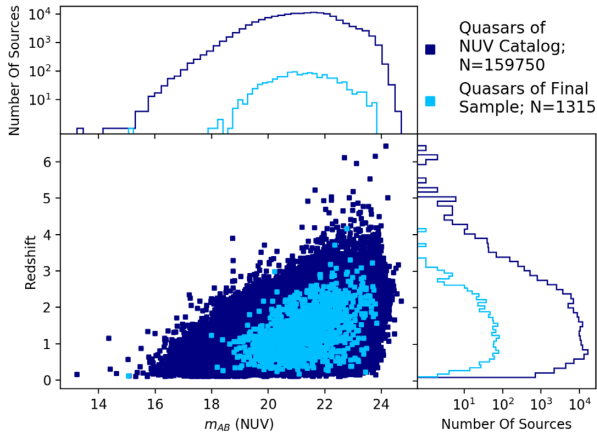


**Figure 3.** The distribution of redshifts and mean NUV magnitudes of 159 750 quasars extracted from *GALEX* (dark blue) and the final sample of 1315 quasars used in our analysis (light blue).

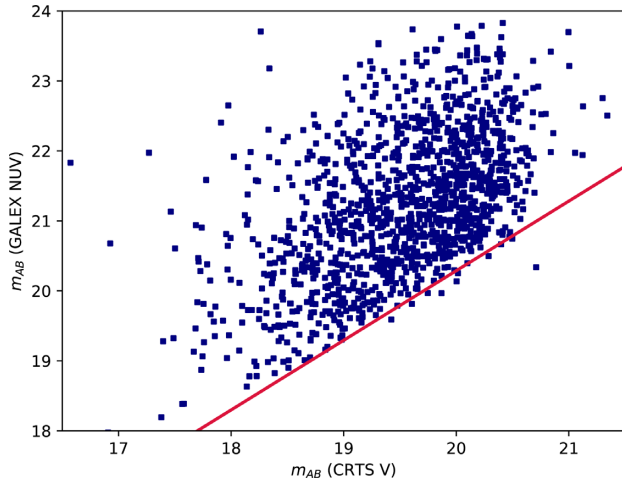


**Figure 4.** Mean photometric optical and NUV magnitudes of the 1315 sources in our final sample. For reference, the diagonal red line shows when the two magnitudes are equal.

sparse light curves. The magnitude distribution is similar to the initial sample, except that sources at the rare faint and bright tails of the distribution are missing from the final sample. For the final sample, we also illustrate the mean NUV magnitude versus the mean V-band magnitude, in Fig. 4. The magnitudes in the two bands are correlated to some extent (i.e. if a source is bright in optical, it is generally also bright in UV, and vice versa), and the optical magnitude is typically brighter than the NUV, as expected from the typical spectral energy distribution of quasars.

## 2.3 Data analysis

### 2.3.1 Observed data

In order to characterize the correlations between optical and UV variability in the sample as a whole, we first quantify the cross-correlation for each of the 1315 sources individually. We first pre-processed the light curves (optical and NUV) removing outliers and binning in 1 d intervals, following the steps in Charisi et al. (2016). Note that the short-term variability is not significant for

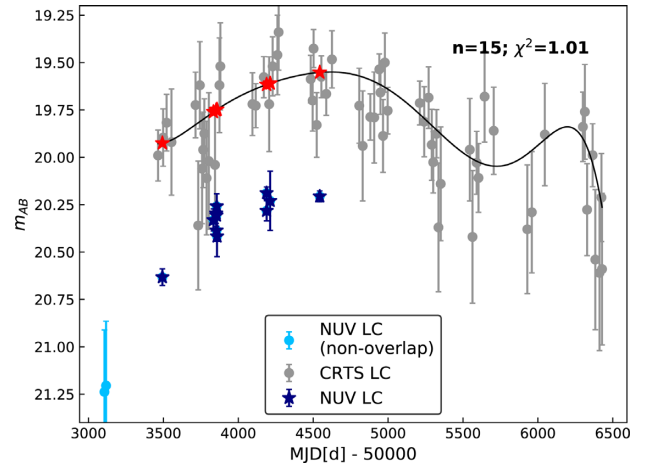


**Figure 5.** This example source, SDSS J125731.3+001454, has an optical light curve (LC; data shown by grey circles with error bars) that is well described by a best-fitting polynomial of order  $n = 15$  with a reduced  $\chi^2 = 1.01$  (black curve). The corresponding UV data points outside and inside the time interval that overlaps with the optical data are denoted by light blue circles and dark blue stars, respectively. The red stars mark the optical data interpolated to the times of the UV observations, using the best-fitting polynomial. The cross-correlation coefficient measured between the red and dark blue stars is  $R = 0.86$ .

the cross-correlation analysis and thus binning does not affect our results.

Calculating cross-correlations with our data is challenging, because the observations in the two bands are not taken simultaneously. To address this, we interpolated the optical light curves with a polynomial. We chose to interpolate the optical light curves, because the quality of the data is significantly higher than in the NUV (i.e. the optical data typically have more epochs, smaller gaps and lower photometric uncertainty). We found the best-fitting polynomial for each binned optical light curve by varying the polynomial order from  $n = 6$  to  $n = 30$ , and choosing the smallest  $n$  that produces a reduced  $\chi^2$  close to unity. This process ensures reasonable fits, while avoiding overfitting.

Fig. 5 illustrates a typical example of a pair of optical and UV light curves, along with the best-fitting polynomial for the optical data (shown with the black line). We computed the cross-correlation coefficient,  $R_i$ , based on the overlapping part of the optical and UV light curves. Even though the polynomial fits are a reasonable fit for the optical light curves, they cannot be extrapolated beyond the range of available data. Therefore, we used only the UV data points whose dates fall inside the optical baseline (stars in dark blue in Fig. 5) and excluded the UV points outside this range (light blue points in Fig. 5). We then selected the points from the polynomial fit that correspond to the times of the UV observations, giving us new optical points (red stars in Fig. 5) that are simultaneous with the UV.

Having calculated the magnitudes at  $N$  coincident times, the standard Pearson cross-correlation coefficient can then be straightforwardly evaluated

$$R_{\mathbf{X}\mathbf{Y}}^2 \equiv \frac{[\text{Cov}(\mathbf{X}, \mathbf{Y})]^2}{[\text{Var}(\mathbf{X})][\text{Var}(\mathbf{Y})]}, \quad (1)$$

where  $\mathbf{X} = (x_1, x_2, \dots, x_N)$  and  $\mathbf{Y} = (y_1, y_2, \dots, y_N)$  represent the optical and UV data vectors, at times  $(t_1, t_2, \dots, t_N)$ . With the above method, we obtained the cross-correlation coefficient  $R_i$  for each of



the 1315 sources and derived the corresponding distribution of the correlation coefficient,  $P(R_{\text{obs}})$ .

### 2.3.2 Modelling and simulations

We performed a theoretical study of the optical/UV variability of the population of quasars to explore whether the observed distribution  $P(R_{\text{obs}})$  reflects genuine correlations.

First, we conducted a null test, in which the optical and UV light curves are completely uncorrelated. For this, we randomly shuffled the pairings of the optical and UV data, i.e. every optical light curve is paired up with the UV light curve from a different quasar, rather than from itself, so that no correlation is expected. We shuffle all of the quasars regardless of their redshift; this is justified because we find that neither the sampling properties, nor the inferred correlations, show any systematic redshift dependence (see Section 4.5 and Fig. 15). We then repeated the calculation of the  $R_i$  for each pair of UV and optical light curves in this shuffled sample, following the steps detailed in Section 2.3.1 and obtained the distribution of  $R_i$  for this null test  $P(R_{\text{null}})$ . The advantage of this test is that it does not make any assumption for the underlying variability, since it uses only observed data.

Next, we explored the level of correlations for the population by generating model light curves with properties (sampling, photometric errors) similar to the observed ones, and performing the same cross-correlation analysis as above.

In particular, we used the DRW model, which provides a successful description of quasar variability in optical and NUV (MacLeod et al. 2010; Zhu et al. 2016). The DRW parameters (the characteristic correlation time-scale  $\tau$ , and the variability amplitude  $\hat{\sigma}$ ) depend on global quasar properties, such as the redshift, the absolute  $i$ -band magnitude and the black hole mass. For each quasar, we estimated the DRW parameters, using equation (7) and table 1 from MacLeod et al. (2010) for the *SDSS*  $r$  band.<sup>6</sup> For this, we extracted the redshift from the HMQ catalogue, and calculated the absolute  $i$ -band magnitude, and from this the black hole mass, following the steps in Charisi et al. (2016). The exception is that for 373 quasars in our final sample, virial mass estimates were available, which we adopted from Shen et al. (2008). This process produced six outliers with unrealistically large virial masses ( $\sim 10^{13-14} M_{\odot}$ ), likely misclassified blazars,<sup>7</sup> which we excluded from the sample (see also 2.2). The estimated DRW parameters are shown in Fig. 6.

With the DRW parameters estimated above, we generated continuous mock light curves, sampled at 1-d intervals. We examined two scenarios: (1) a perfect correlation between optical and UV variability. In this case, the UV light curve is a rescaled version of the optical, with the relative amplitude  $r_q \equiv \sigma_{\text{opt}}/\sigma_{\text{UV}}$  assumed to be a free parameter. (2) the optical and UV data are not fully correlated. For this, we assumed that a fraction of quasars  $f_{\text{cor}}$  have fully correlated optical–UV variations, while the remaining  $(1 - f_{\text{cor}})$  have uncorrelated variations in the two bands (see also Section 4.2). For the uncorrelated sources, we generated random realization of the optical and UV light curves independently.

We downsampled the continuous DRW light curves generated above, at the observational times by *CRTS* and *GALEX*, respectively. We added Gaussian deviates with zero mean and standard deviation

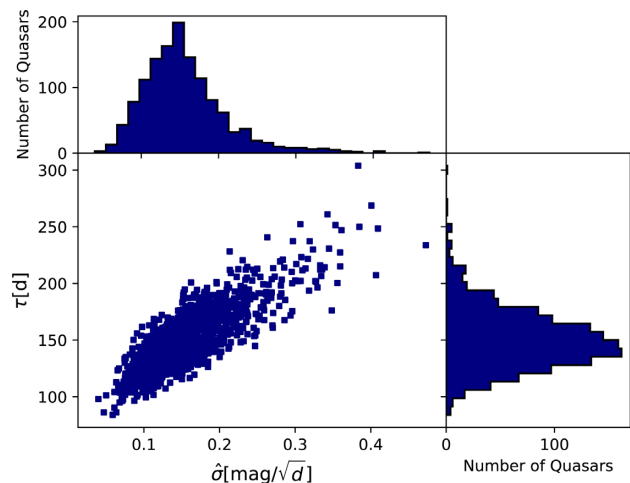


**Figure 6.** DRW model parameters for the sample of 1315 quasars estimated from their properties adopting correlations from MacLeod et al. (2010).

equal to the photometric uncertainty of each point to incorporate the measurement errors. By preserving the observed properties in the simulated light curves, we account for systematic effects introduced by the quality of the data. From the downsampled optical and UV light curves, we calculated the cross-correlation, as before, by interpolating the optical light curve with an  $n^{\text{th}}$ -order polynomial, finding the overlapping interval and selecting the times that correspond to the UV observations. We repeated the process for the entire population, and we obtained the distribution  $P(R_{\text{model}})$ .

Our analysis has two free parameters, the relative amplitude of variability  $r_q$ , which we allowed to vary from 0.5 to 4.5 and the correlated fraction  $f_{\text{cor}}$ , which we varied between 0 and 100 per cent. We sampled the two parameters on an equally spaced  $20 \times 20$  grid in this two-dimensional parameter space. For each pair of  $(f_{\text{cor}}, r_q)$ , we generated 20 independent realizations of the population, resulting in 20 independent  $P(R_{\text{model}})$  distributions for each of the  $20 \times 20 = 400$  pairs of  $(f_{\text{cor}}, r_q)$ .

We compared the simulated realizations  $P(R_{\text{model}})$  with the observed  $P(R_{\text{obs}})$ , using the Kolmogorov–Smirnov test (KS test). In particular, we computed the KS distance ( $D_{\text{KS}}$ ) between the normalized cumulative distribution function (CDF) of  $R_{\text{obs}}$  and each  $R_{\text{model}}$ . This provided 20  $D_{\text{KS}}$  values for each pixel on the  $(f_{\text{cor}}, r_q)$  plane. We used the average,  $\overline{D_{\text{KS}}}$ , as the figure-of-merit to determine which set of parameters better reproduces the observed distribution, with lower values corresponding to better fits to the data.

## 3 RESULTS

We calculated the cross-correlation coefficient for the population of 1315 quasars in our final sample. In Fig. 7, we show the distribution of cross-correlation coefficients  $R_i$  for the observed data  $P(R_{\text{obs}})$  with a solid grey histogram. The distribution shows a clear trend towards large  $R_{\text{obs}}$  values, with a broad peak at  $0.75 \lesssim R_{\text{obs}} \lesssim 1$ .

We then performed a model-independent null test, shuffling the optical and UV pairs of light curves. The distribution of  $R_i$  for this null test  $P(R_{\text{null}})$  is shown by the blue hatched histogram in Fig. 7. We see that in the limit of no correlation, the distribution  $P(R_{\text{null}})$  is relatively flat for all values of  $R_i$ . In the ideal case, a delta function at  $R = 0$  would be expected, but the sparse data flatten the distribution; we further explore the systematics introduced by the limited data quality in Section 4.1.

<sup>6</sup>The *SDSS*  $r$  band is the closest to Johnson  $V$  band, in which the *CRTS* data are calibrated.

<sup>7</sup>The estimation of the black hole mass from the  $i$ -band luminosity from Shen et al. (2008) and MacLeod et al. (2010) does not hold for blazars.

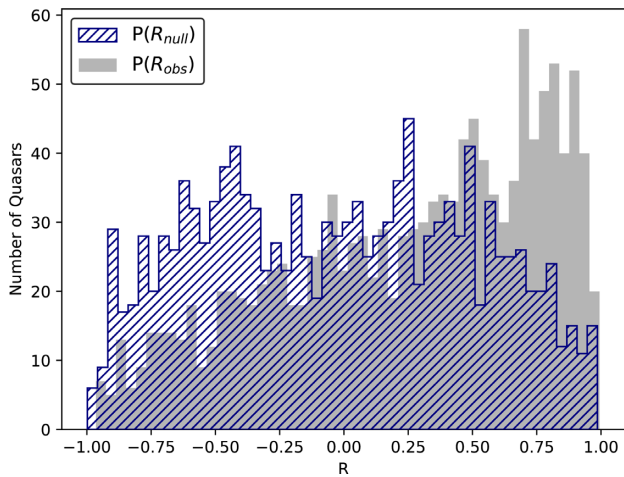


**Figure 7.** Distribution of the cross-correlation coefficient  $R_{\text{obs}}$  between the optical and UV variability in our sample of 1315 quasars (grey). The hatched histogram shows the same distribution obtained from a null test, in which the optical and UV light curve pairings were randomly shuffled, so that no correlations are expected. The comparison between the two histograms reveals that the correlations in the data are genuine and are not produced by poor data quality alone.

The excess of values at the positive correlation end in the observed distribution  $P(R_{\text{obs}})$  compared to the flat  $R_{\text{null}}$  distribution is a strong indication that the optical and UV variability is positively correlated in our sample. In other words, although the suboptimal quality of data (e.g. due to sparse sampling, significant photometric errors, non-simultaneous observations, etc.) may smear the apparent  $R$ -distribution, they do not, by themselves account for the skewed observed shape in  $P(R_{\text{obs}})$ .

Next, we compared the observed distribution  $P(R_{\text{obs}})$  with theoretical distributions produced from simulated light curves  $P(R_{\text{model}})$ . In Fig. 8, we show model distributions, assuming that the optical and UV variability are fully correlated (scenario 1), while varying the relative amplitude of variability  $r_q$ . We see that the simulated distributions begin to approach the observed one as the variability amplitude is increased, with  $r_q$  between 1.5 and 2.5 providing the best fit. For even larger  $r_q$ , the simulated histograms show overly skewed positive correlations. This is expected: as the UV variability stands out more above the noise, the intrinsic correlations show up more accurately in the measurements. The best-fitting values of  $1.5 \lesssim r_q \lesssim 2.5$  are consistent with previous studies, which showed that quasars tend to have higher variability amplitudes at shorter wavelengths (Welsh et al. 2011; Gezari et al. 2013; Zhu et al. 2016; Charisi et al. 2018). Another important feature is that none of the model distributions for fully correlated variability can reproduce the observed distribution exactly; there is always an excess of  $R_i$  at negative values ( $R < 0$ ).

The above finding led us to explore scenario B, in which we vary the fraction of quasars that are fully correlated  $f_{\text{cor}}$  for a fixed variability amplitude. We chose  $r_q = 2.5$ , since, as seen in Fig. 8, this variability amplitude provides a relatively good fit to the observed distribution. The resulting distributions are shown in Fig. 9.<sup>8</sup> As this figure shows, for  $f_{\text{cor}} \approx 60$  per cent, the simulated distribution  $P(R_{\text{model}})$  appears consistent with the observed  $P(R_{\text{obs}})$ , whereas for

higher/lower values of  $f_{\text{cor}}$ , it becomes too steep or missing the peak near  $R \approx 1$ , respectively.

The above two figures demonstrate the need to fully explore the parameter space, considering both the fraction of quasars that are fully correlated  $f_{\text{cor}}$  and the amplitude ratio between stochastic UV and optical variability  $r_q$  as free parameters. For each pair of  $(f_{\text{cor}}, r_q)$ , we generated 20 random realizations of the population and calculated the KS distance for each. In Fig. 10, we present our figure-of-merit, i.e. the average (from 20 realizations) KS distance between the modelled and the observed  $R$ -distributions ( $\overline{D}_{\text{KS}}$ ), over our 2D parameter space. The colour bar on the right side of the figure indicates different values of  $\overline{D}_{\text{KS}}$ . The yellow contour on this 2D grid encloses all pixels which had the lowest  $\overline{D}_{\text{KS}}$  in any one of the 20 realizations. These represent the set of models which were found to be best-fitting models (i.e. the combination of parameters that returned the lowest  $\overline{D}_{\text{KS}}$ ) in any of our 20 realizations.<sup>9</sup> We interpret this region as our 95 per cent confidence region (i.e. the chance that the best-fitting model falls outside this region is  $\lesssim 5$  per cent).

Since Fig. 10 focuses on the average KS distance and does not show the distribution of values from the individual realizations, in Fig. 11, we show the figure-of-merit  $\overline{D}_{\text{KS}}$  as a function of  $f_{\text{cor}}$  at fixed  $r_q$ , with error bars that represent the full range of values we obtained from the 20 realizations. Red triangles, blue circles, and green squares illustrate  $r_q = 1.1, 2.5$ , and 4.1, respectively. The relatively small error bars demonstrate that the observed minima are real and the observed trends are not sensitive to individual random realizations of the population. As a result, the trend and peaks we see in Fig. 10 are robust.

Overall, the figure-of-merit based on the KS test shows a well-defined peak at  $(f_{\text{cor}}, r_q) \approx (60 \text{ per cent}, 2.5)$ , representing the best-fitting parameter values, for which the predicted  $R$ -distribution is closest to the one observed. This corresponds to a simple model in which the UV *versus* optical DRW amplitude ratio is always 2.5, and in which 60 per cent of all quasars have fully correlated UV *versus* optical variability (with  $R = 1$ , otherwise  $R = 0$ ). This model provides a good match to the observed  $R$ -distributions.

A corollary of our finding is that the simplest scenario, in which all quasars have well-defined correlations between optical and UV variability, as may have been inferred from prior studies on a small sample of  $\sim$  two dozen AGNs, is ruled out by our analysis at high confidence. We note however that in our analysis we simulated a population with a fixed constant variability amplitude  $r_q$ . It is possible that if we varied  $r_q$ , we could reproduce the observed distribution  $R_{\text{obs}}$ , even for fully correlated light curves. We will explore this case in future work.

## 4 DISCUSSION

### 4.1 Sampling and photometric errors

The null test of completely uncorrelated optical and UV variability returned a flat distribution  $R_{\text{null}}$ . Ideally, we should infer a distribution similar to a delta function, with a peak at  $R = 0$ . This means that the limited data quality can introduce spurious cross-correlations ( $R \neq 0$ ). This could potentially be improved, if the light curves were sampled at higher cadence, had smaller photometric errors, or longer baselines. Here, we examine the impact of these three aspects.

<sup>8</sup>We did not reproduce the case with  $f_{\text{cor}} = 100$  per cent in Fig. 9 – this is the same as the middle panel in Fig. 8, where all quasars have fully correlated optical and UV variability.

<sup>9</sup>There are fewer than 20 pixels inside this contour, because two or more realizations sometimes yield the same best-fitting pixel.

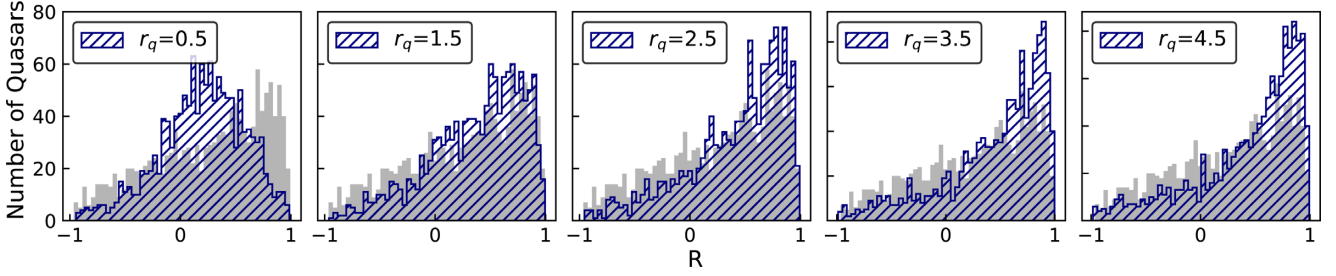


**Figure 8.** Distributions of the cross-correlation coefficient  $P(R_{\text{model}})$  assuming fully correlated UV and optical data (blue hatched histograms), for different amplitude ratios,  $r_q$ , compared to the observed distribution (grey; same in every panel).

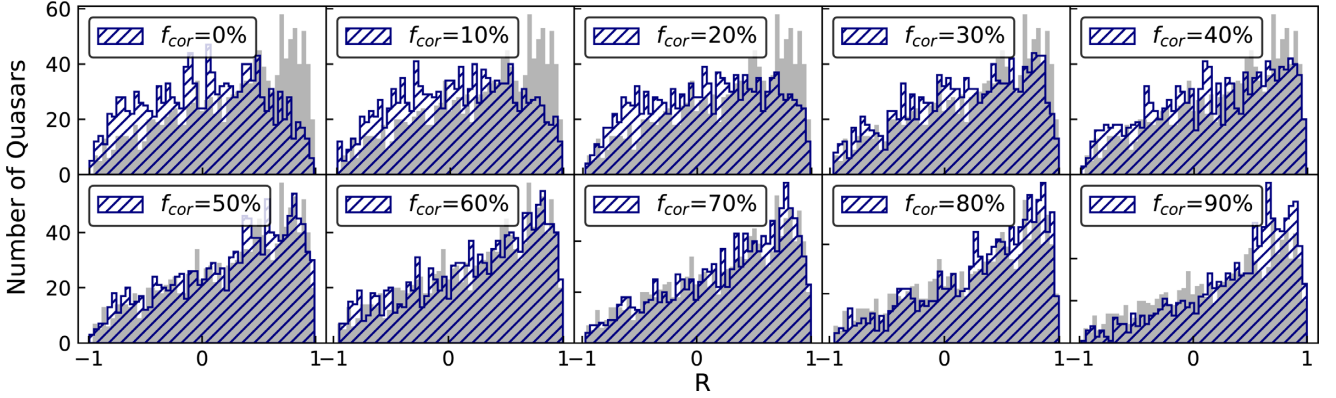


**Figure 9.** Distributions of the cross-correlation coefficient  $R_{\text{model}}$  predicted for different correlated fractions  $0 \leq f_{\text{cor}} \leq 90$  per cent at fixed variability amplitude ratio  $r_q = 2.5$  (blue hatched), compared to the observed distribution (grey; same in every panel).

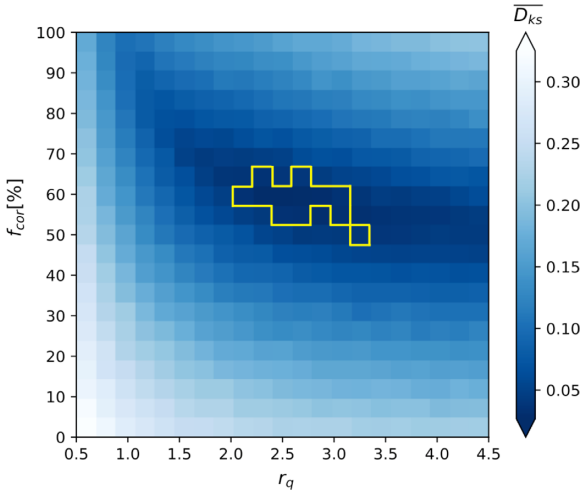


**Figure 10.** Average KS distance,  $\overline{D_{\text{KS}}}$ , as a function of the fraction of fully correlated quasars,  $f_{\text{cor}}$ , and amplitude ratio of UV-to-optical DRW variability,  $r_q$ . The yellow contour marks an estimate of the 95 per cent confidence region.

First, we explored systematics from the limited quality of the UV light curves, generating simulations of uncorrelated light curves ( $R = 0$ ), with a fixed variability amplitude ratio at  $r_q = 2.5$  (as in Fig. 9). In order to understand the effect of photometric errors of the UV simulated light curves, we set the photometric errors to zero (practically, we generated noiseless DRW light curves), and kept the original cadence and baseline of the observations. The resulting distribution is shown by the grey histogram in the top

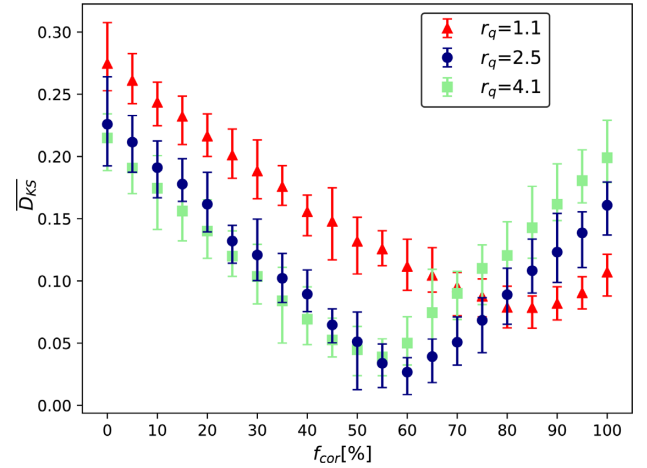


**Figure 11.** Average KS distance  $\overline{D_{\text{KS}}}$  and error bars (representing the full range of  $D_{\text{KS}}$  over 20 realizations) as a function of  $f_{\text{cor}}$  for  $r_q = 1.1, 2.5$ , and  $4.1$  (as labelled in the inset).

panel of Fig. 12. For reference, we also show the distribution, in which the photometric errors were included in the simulations in blue; this is the same as the top left panel of Fig. 9. The distributions (from simulations with and without UV photometric errors) are very similar, which indicates that the photometric errors have a negligible effect and are not the main culprit for flattening the  $R$ -distribution. The only visible differences appear near  $R \approx \pm 1$ : the addition of purely random noise in the UV time series makes it less probable for such strong (anti)correlations to arise by chance.



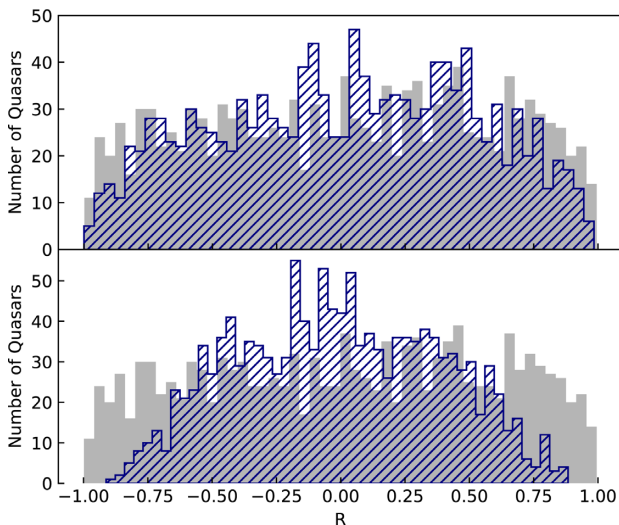


**Figure 12.** Distributions of the cross-correlation coefficients (solid grey; same in both panels) of mock optical and UV data sets, assuming uncorrelated DRW variability in the two bands (true  $R = 0$ ), noise ratio  $r_q = 2$ , and no photometric errors. The dark blue hatched histogram in top panel denotes the distribution obtained from 10 times more densely sampled UV time series, whereas the hatched histogram in the bottom shows the distribution with the photometric errors included (same as the last panel with  $f_{\text{cor}} = 0$  in Fig. 9).

Then, we explored the effect of sampling, generating high-cadence mock UV light curves. For this, we inserted nine additional data points, spaced evenly between each two consecutive observed times, such that the resulting UV MJDs are 10 times more densely sampled. We downsampled the mock DRW light curves at the new UV MJDs to obtain UV light curves with higher cadence and no photometric errors. This new sample yields the blue hatched histogram at the bottom panel of Fig. 12. As the figure shows, the gains are relatively modest, and the expected delta function at  $R = 0$  remains highly smeared out, despite the 10-fold increase in the density of the UV time series.

Finally, we explored a more idealized case. We generated optical and UV DRW time series with 1-d cadence, and with the same baselines (i.e. the baselines of the optical DRW light curves) in the two bands. We repeated these idealized simulations with extended baselines of either 5 or 10 times their original optical baselines. The three distributions are shown in Fig. 13, where  $P(R_{\text{BL}}^{\text{RW}})$  (light blue) shows the case, where the length of the DRW light curves is fixed at the observed value of the initial optical light curves plus  $P(R_{5 \times \text{BL}}^{\text{RW}})$  (medium) and  $P(R_{10 \times \text{BL}}^{\text{RW}})$  (dark) show the distributions for the extended light curves with  $5 \times$  and  $10 \times$  longer baselines, respectively. The light blue distribution shows a significant improvement compared to the dark blue distribution in Fig. 12, which means that the even denser and coincident sampling both for the optical and UV light curves reduces the chance of detecting correlations by chance. However, the distribution is still relatively broad. As can be seen from Fig. 13, the distributions obtained from DRWs with longer baselines converge more closely to the expected delta function.

## 4.2 Partial correlations

We tested a simple scenario, in which a fraction of quasars are fully correlated and the rest have fully uncorrelated UV and optical variability. In general, there could be different levels of

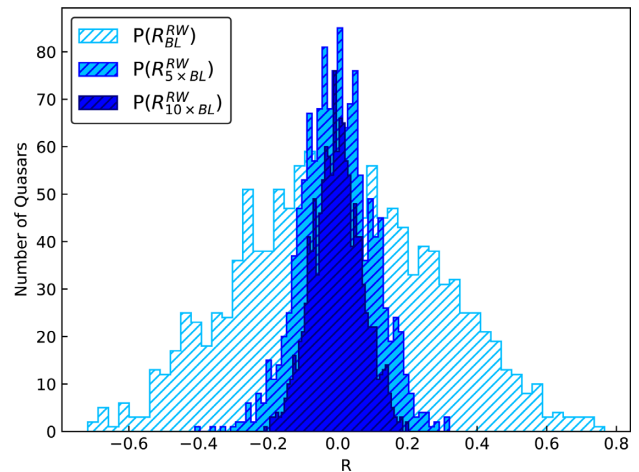


**Figure 13.** Probability distributions of the cross-correlation coefficients of DRW optical and UV data sets with different baselines, assuming uncorrelated DRW variability in the two bands (true  $R = 0$ ) and noise ratio  $r_q = 2.5$ . The light blue histogram denotes the distribution obtained from DRW data sets with the same baselines as the *CRTS* light curves. The medium and dark blue histograms show distributions where the baselines in DRW data sets are 5 and 10 times longer, respectively.

partial optical–UV correlations, and this level can be different from one source to another, i.e. each quasar could have a partially correlated optical–UV variability with  $R \in [0, 1]$ . In fact, this already seems to be the case for the well-sampled light curves in Edelson et al. (2019). We calculated the cross-correlation coefficients for these sources between the *V* and *M2* bands<sup>10</sup> light curves (NGC 4151,  $R = 0.81$ ; NGC 5548,  $R = 0.92$ ; NGC 4593,  $R = 0.62$ ; Mrk 509,  $R = 0.97$ ). Note that, since these light curves are well-sampled, for this calculation we omitted the polynomial interpolation of the optical light curve, which likely introduces additional biases. The correlation coefficients of these light curves indicate that partially correlated UV/optical variability exists (i.e.  $R \neq 1$ ) even with well-sampled light curves. This suggests that the partial correlations found in our sample are unlikely to arise solely from the poor sampling of UV light curves. We intend to address the role of intrinsic partial correlations in a future analysis.

In this paper, we focused on testing the first hypothesis (a fraction of quasars have fully uncorrelated data), which is the simplest to implement. However, given the quality of the data, we expect that the two cases will likely produce indistinguishable distributions. While we will not evaluate the second case here, we defer to future work to assess how well a population of quasars with partially correlated light curves fits the same data analysed here. This can be attained by generating pairs of mock DRW light curves whose input is  $R < 1$ .

## 4.3 Time delays

If the UV/optical luminosity arises via reverberation of a central illuminating source, the variability should track one another, but with a time delay that corresponds to their relative distances to the central source. Typical delays are expected to be of the order of days (see e.g. Edelson et al. 2019 and references therein). Even for the

<sup>10</sup>The *M2* band is the closest to *GALEX* NUV.



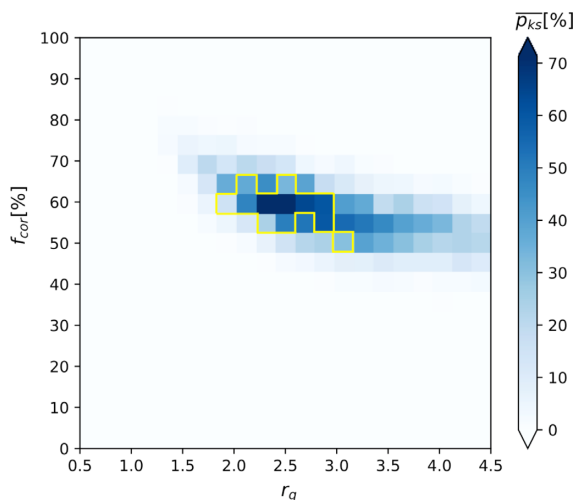


**Figure 14.** Average KS probability from 20 realizations for each pixel as a function of the fraction of quasars  $f_{\text{cor}}$  and the variability amplitude  $r_q$ . The yellow contour indicates the 95 per cent confidence level (same as the yellow contour in Fig. 10).

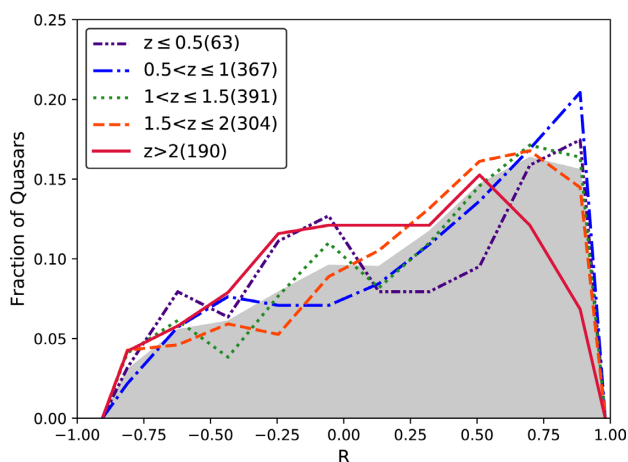


**Figure 15.** The (normalized) distribution of the cross-correlation coefficient  $R$ , computed among quasars in five distinct redshift bins as labelled in the inset panel. The numbers in parentheses indicate the number of quasars within the corresponding bin. The  $R$ -distribution of the entire sample is superimposed (grey).

massive quasars in our sample, with SMBH mass of  $\sim 10^9 M_\odot$  the light-crossing time is  $\sim 12$  d, given the expected size of the optical emission, which is  $\sim 100 R_s$ , where  $R_s$  is the Schwarzschild radius. Observationally, the size of the optical emission region is smaller (e.g. fig. 1 in Morgan et al. 2007 shows  $< 10^{16}$  cm, corresponding to a light-crossing time of  $\sim 4$  d).

Our data are not sufficiently well sampled to be sensitive to these short delays. We verified this expectation by simulating optical and UV light curves with time lags between 1 and 100 d and repeating our analysis. For the simulations here, we adopted  $f_{\text{cor}} = 60$  per cent and  $r_q = 2.5$ . We calculated the average KS distance and found no significant difference. We concluded that more densely sampled light curves are necessary to probe time lags expected in reverberation models of thin discs.

#### 4.4 KS probability

In our analysis above, we quantified how well a model distribution fits the observed data using the KS distance. In the standard version of the KS test, the KS distance corresponds to a probability that the examined distribution is drawn from a reference distribution. In our case, this can be loosely translated into the likelihood that our distribution  $R_{\text{obs}}$  was drawn from the predicted probability distribution  $R_{\text{model}}$ . However, the results need to be interpreted with caution, since the assumptions do not obey the formal requirements to convert the KS distance to probability. In particular, the  $R_i$  values are not drawn independently from the same distribution, because each  $R_i$  is calculated for a different quasar. Since the properties of the individual pairs of light curves are not dramatically different, the obtained probabilities should be approximately correct. With this caveat in mind, for each realization of the population presented in Fig. 10, we calculated the KS probability. In Fig. 14, we show the average probability ( $\overline{p_{\text{KS}}}$ ) for each of the  $20 \times 20$  pixels on the ( $f_{\text{cor}}$ ,  $r_q$ ) plane. We see that this figure delineates a similar region as the 95 per cent contour we identified in Fig. 10, providing additional justification for identifying this as our 95 per cent confidence region.

#### 4.5 The effect of redshift

As mentioned in Section 1, all of our analysis was performed in the observer frame. Fig. 3 shows that our final sample spans a small, but significant range of redshifts, with the majority of quasars between  $0.3 \lesssim z \lesssim 2.5$ . Since we are probing different rest-frame emission from quasars at different redshifts, this could impact our results, if the optical–UV correlations were strongly dependent on the exact rest-frame wavelength within either band.

As an example, assuming blackbody radiation from a standard thin Shakura–Sunyaev disc, the effective temperature, as well as the (inverse) rest-frame wavelength of the peak of the emission, scale with distance from the central SMBH as  $T \propto \lambda_r^{-1} \propto r^{-3/4}$ . As a result, at fixed observed wavelength  $\lambda_{\text{obs}} = (1+z)\lambda_r$ , the characteristic radius of emission scales as  $r \propto [\lambda_{\text{obs}}/(1+z)]^{4/3} \propto (1+z)^{-4/3}$ . This implies that we are probing more compact regions of the discs of higher redshift quasars, with the difference as much as a factor of  $\sim 3$ –4 between the lowest and highest redshift quasars in our sample. It is plausible that these different parts of the disc exhibit different correlations.

In addition, the redshift could have an effect on the time delay between UV and optical luminosity. Since time delays are associated with the relative sizes and distances of the UV and optical emission regions from the central SMBH, time delays at higher redshifts are expected to be shorter. This is counterbalanced by the redshift time dilation. As discussed above, the time delays are not expected to strongly affect our results, especially given the sparse light curves. Therefore, we expect a weak impact of the redshift-dependent time delays on the inferred cross-correlations.

In order to assess the effect of redshift on our results, we examined how our results depend on quasar redshift. We divided our sample into five narrower redshift bins, and computed the distribution of the cross-correlation coefficient  $R$  in each bin. The results are shown in Fig. 15. The distributions are noisier, due to the smaller number of quasars in each narrow  $z$ -bin, but overall, these distributions do not show a systematic trend with redshift. This serves as a reassurance that our main results are not strongly impacted by mixing different redshifts (or correspondingly different disc regions). On the other hand, there does appear to be fewer highly correlated cases ( $R \gtrsim 0.8$ ) in the two highest redshift bins. This could be explained from the

reduced data quality of this subsample. Generally, quasars appear dimmer at high redshift (see Fig. 3) and as a result, they have lower quality data with larger photometric errors. This tends to eliminate the strongest correlations (as shown in the bottom panel of Fig. 12). This may help explain why we find a lack of strongly correlated sources in the highest redshift bins in Fig. 15. This trend could have an impact on the overall correlation distribution, requiring a smaller  $f_{\text{cor}}$ , but given that the  $z > 2$  bin contains a relatively small number of quasars, we expect that it would not significantly alter our conclusions.

#### 4.6 Future work

One caveat in our hypothesis testing is that throughout the analysis we assumed that the intrinsic variability in both the optical and UV bands follows the statistics of the DRW model. As mentioned in the Introduction, there is evidence that this phenomenological model does not fully describe quasar variability in the optical bands. A full investigation of other stochastic variability models is beyond the scope of this paper. Nevertheless, we expect that departures from the DRW model could affect our results. In particular, if the true intrinsic variability is weakly correlated compared to the expectation from the DRW model (e.g. approaches white noise), this could reduce cross-correlations arising by chance between the two bands. This is because in correlated variability, if we assume stronger correlations, the flux of the subsequent observations strongly depends on the previous data points. In turn, this could increase the level of genuine intrinsic cross-correlations required to match the values we inferred here from the observations. Future work should assess the validity of our findings by exploring more advanced stochastic variability models.

Another major limitation in our study is presented by the quality of the data. In particular, the UV light curves are available for a limited number of sources and they are typically characterized by a small number of observations, large gaps, etc. Here, we attempted the most extensive analysis of optical and UV data, combining data from two massive time-domain surveys in optical and UV (*CRTS* and *GALEX*, respectively). The UV/Optical Telescope (UVOT) on board the Neil Gehrels *Swift* Observatory provides useful additional UV data, which can enhance the *GALEX* light curves, especially since the *GALEX* NUV band and the *Swift* M2 band have very similar wavelength coverage.<sup>11</sup> Similarly, in optical bands, there are several time-domain surveys, such as the Zwicky Transient Facility (ZTF), the Panoramic Survey Telescope and Rapid Response System (Pan-STARRS), and the All-Sky Automated Survey for Supernovae (ASAS-SN), and in the near-future the Large Survey of Space and Time (LSST). It would be beneficial to combine data from multiple time-domain surveys, both in optical and UV, in order to achieve the highest quality light curves, while maintaining a sizeable sample. This will require a significantly more complex analysis, addressing cross-calibrations between different data sets, and combining heterogeneous individual observations, we leave this to future work.

## 5 CONCLUSIONS

In this paper, we performed a study of the correlation between observed UV and optical variability of quasars. These interband

correlations are a useful probe of the physics of accretion discs in quasars, but they are challenging to measure, mostly because time-domain data in the UV are sparse. As a result, previous studies focused on a handful of quasars with targeted observations and well-sampled light curves in both bands; they found strongly correlated variability. Here we complemented previous studies and instead assembled a large sample of 1315 quasars, which were selected from HMQ by requiring that they have spatially and temporally overlapping time-domain data in both *GALEX* and *CRTS*. Note that the assumption that all parent sources in the HMQ are indeed quasars depends on the accuracy of HMQ source classification, and, inevitably, so do our conclusions. While this necessitated a compromise in the data quality for the individual light curves, we were able to analyse this sample statistically, and extract the intrinsic correlations between the optical and UV light curves for the population as a whole. Our analysis utilized mock light curves, which mimic the important features of the data (such as sampling, baseline, and photometric errors). We also performed a model-independent null test, in which we random shuffled the pairings of the optical *versus* UV light curves.

We found that strong correlations exist in this much larger sample, but we ruled out, at  $\sim 95$  per cent confidence, the simple hypothesis that the intrinsic UV and optical variations of all quasars are fully correlated. We explored a simple model, in which a fraction  $f_{\text{cor}}$  of quasars have UV light curves that are fully correlated with the optical, but with an amplitude that is scaled by a factor of  $r_q$ , while the remaining fraction  $(1 - f_{\text{cor}})$  are not correlated at all. We found that the values of  $f_{\text{cor}} \approx 60$  per cent and  $r_q \approx 2.5$  best reproduce the observed distribution of correlation coefficients. Therefore, our results imply the existence of physical mechanism(s) that can generate uncorrelated optical and UV flux variations, such as expected, for example, from local temperature fluctuations (Dexter & Agol 2011).

Future work should extend our analysis, by improved modelling of intrinsic quasar variability, and allowing for partially correlated UV *versus* optical fluctuations. Our study was also limited by the available UV data, ultimately resulting in a cut from  $\sim 150\,000$  quasars down to a sample of  $\sim 1000$  with sufficient overlapping optical and UV data. A future UV time-domain survey would yield great improvements. Our analysis in Section 4, especially Fig. 13, further indicates that apart from the number of sources, the main limitation for our study was the length of the baseline: the best improvement would be provided by a large-area UV and optical surveys with simultaneous observations covering at least several years.

## ACKNOWLEDGEMENTS

We thank Suvi Gezari for helpful discussions, Rick Edelson for providing the *Swift* light curves, and the anonymous referee for useful comments that improved this manuscript. We acknowledge support from NASA through Astrophysics Data Analysis Program (ADAP) grant 80NSSC18K1093 (to ZH and DS) and through *Swift* grant 80NSSC19K0149 (ZH and MC), and from the National Science Foundation (NSF) through AST grant 1715661 (ZH) and through the North American Nano-hertz Observatory for Gravitational Waves (NANOGrav) Physics Frontier Center, award number 1430284 (MC). The CSS survey is funded by the National Aeronautics and Space Administration under Grant No. NNG05GF22G issued through the Science Mission Directorate Near-Earth Objects Observations Program. The *CRTS* survey is supported by the U.S. National Science Foundation under grants AST-0909182 and AST-1313422.

<sup>11</sup> *Swift* UVOT data have been used in optical/UV variability studies to date focusing only on well-sampled light curves of targeted sources (e.g. Edelson et al. 2019).

## REFERENCES

- Andrae R., Kim D. W., Bailer-Jones C. A., 2013, *A&A*, 554, 1
- Bianchi L., Shiao B., Thilker D., 2017, *ApJS*, 230, 24
- Charisi M., Bartos I., Haiman Z., Price-Whelan A. M., Graham M. J., Bellm E. C., Laher R. R., Márka S., 2016, *MNRAS*, 463, 2145
- Charisi M., Haiman Z., Schiminovich D., D’Orazio D. J., 2018, *MNRAS*, 476, 4617
- D’Orazio D. J., Haiman Z., MacFadyen A., 2013, *MNRAS*, 436, 2997
- D’Orazio D. J., Haiman Z., Schiminovich D., 2015, *Nature*, 525, 351
- Dexter J., Agol E., 2011, *ApJ*, 727, 1
- Drake A. J. et al., 2009, *ApJ*, 696, 870
- Edelson R. et al., 2019, *ApJ*, 870, 123
- Farris B. D., Duffell P., MacFadyen A. I., Haiman Z., 2014, *ApJ*, 783, 12
- Fausnaugh M. M. et al., 2016, *ApJ*, 821, 56
- Flesch E. W., 2015, *Publ. Astron. Soc. Aust.*, 32, e010
- Frank J., King A., Raine D. J., 2002, *Accretion Power in Astrophysics*. Cambridge Univ. Press, Cambridge
- George I. M., Fabian A. C., 1991, *MNRAS*, 249, 352
- Gezari S. et al., 2013, *ApJ*, 766, 60
- Graham M. J. et al., 2015, *MNRAS*, 453, 1562
- Hayasaki K., Mineshige S., Ho L. C., 2008, *ApJ*, 682, 1134
- Hung T. et al., 2016, *ApJ*, 833, 226
- Ivezic Z., MacLeod C. L., 2013, *Multiwavelength AGN Surveys and Studies, Proc. IAU Symp. 304*. Kluwer, Dordrecht, p. 11
- Kelly B. C., Bechtold J., Siemiginowska A., 2009, *ApJ*, 698, 895
- Kokubo M., 2015, *MNRAS*, 449, 94
- Kokubo M., Morokuma T., Minezaki T., Doi M., Kawaguchi T., Sameshima H., Koshida S., 2014, *ApJ*, 783, 46
- Kozłowski S., 2017, *A&A*, 597, A128
- Kozłowski S. et al., 2010, *ApJ*, 708, 927
- Krolik J. H., Horne K., Kallman T. R., Malkan M. A., Edelson R. A., Kriss G. A., 1991, *ApJ*, 371, 541
- Li S.-L., Cao X., 2008, *MNRAS*, 387, L41
- Liu T., Gezari S., Miller M. C., 2018, *ApJ*, 859, L12
- Lynden-Bell D., 1969, *Nature*, 223, 690
- MacFadyen A. I., Milosavljević M., 2008, *ApJ*, 672, 83
- MacLeod C. L. et al., 2010, *ApJ*, 721, 1014
- Martin D. C. et al., 2005, *ApJ*, 619, L1
- Morgan C. W., Kochanek C. S., Morgan N. D., Falco E. E., 2007, *ApJ*, 712, 1129
- Muñoz D. J., Miranda R., Lai D., 2019, *ApJ*, 871, 84
- Pereyra N. A., Vanden Berk D. E., Turnshek D. A., Hillier D. J., Wilhite B. C., Kron R. G., Schneider D. P., Brinkmann J., 2006, *ApJ*, 642, 87
- Roedig C., Dotti M., Sesana A., Cuadra J., Colpi M., 2011, *MNRAS*, 415, 3033
- Ruan J. J., Anderson S. F., Dexter J., Agol E., 2014, *ApJ*, 783, 105
- Sánchez-Sáez P., Lira P., Mejía-Restrepo J., Ho L. C., Arévalo P., Kim M., Cartier R., Coppi P., 2018, *ApJ*, 864, 87
- Schmidt K. B., Rix H. W., Shields J. C., Knecht M., Hogg D. W., Maoz D., Bovy J., 2012, *ApJ*, 744
- Shen Y., Greene J. E., Strauss M. A., Richards G. T., Schneider D. P., 2008, *ApJ*, 680, 169
- Shi J.-M., Krolik J. H., Lubow S. H., Hawley J. F., 2012, *ApJ*, 749, 118
- Smith K. L., Mushotzky R. F., Boyd P. T., Malkan M., Howell S. B., Gelino D. M., 2018, *ApJ*, 857, 141
- Vanden Berk D. E. et al., 2004, *ApJ*, 601, 692
- Welsh B. Y., Wheatley J. M., Neil J. D., 2011, *A&A*, 527, A15
- Wilhite B. C., Vanden Berk D. E., Kron R. G., Schneider D. P., Pereyra N., Brunner R. J., Richards G. T., Brinkmann J. V., 2005, *ApJ*, 633, 638
- Xin C., Charisi M., Haiman Z., Graham M. J., Stern D., D’Orazio D. J., Schiminovich D., 2019, *MNRAS*, 11, 1
- Zhu F.-F., Wang J.-X., Cai Z.-Y., Sun Y.-H., 2016, *ApJ*, 832, 75

This paper has been typeset from a  $\text{\LaTeX}$  file prepared by the author.